Theoretical Study of the Regioselectivity of [2 + 2] Photocycloaddition Reactions of Acrolein with Olefins

Pablo Jaque,*,† Alejandro Toro-Labbé,‡ Paul Geerlings,† and Frank De Proft*,†

Eenheid Algemene Chemie, Faculteit Wetenschappen, Vrije Universiteit Brussel (VUB), Pleinlaan 2, Brussels, Belgium, and Laboratorio de Química Teórica Computacional (QTC), Facultad de Química, Pontificia Universidad Católica de Chile, Casilla 306, Correo 22, Santiago, Chile

Received: September 1, 2008; Revised Manuscript Received: October 17, 2008

The regioselectivity of the [2 + 2] photocycloaddition reaction between triplet $\pi\pi^*$ acrolein and substituted olefins in their ground states was studied using the reaction force concept and reactivity indices from conceptual spin-polarized density functional theory. In the first part, the reaction path was determined for the attack of the acrolein α- and β-carbon atoms on the alkenes, yielding biradical intermediates evolving to the head-to-tail (**HT**) and head-to-head (**HH**) regioisomers, respectively. The β pathway was found to be the most favorable path from the thermodynamic and kinetic points of view, indicating that the formation of the **HH** cycloadduct should be preferred for reactions with both electron-rich and electron-poor alkenes if this first step determines the final regioselectivity. In the second part, the reactivity of the biradical intermediates was characterized through global and local spin-polarized response functions, together with the local hard−soft acid−base principle. The results indicate that the intermediate formed from the electron-rich alkenes evolves preferentially toward the **HT** regioisomer whereas electron-poor alkenes tend to form the **HH** isomer, in agreement with experiment and previous theoretical studies.

1. Introduction

An understanding of the origin of the preference for one bond-making and -breaking path over others in a chemical reaction plays a key role in chemical synthesis. A deeper insight into the factors favoring a given reaction path can lead to an improved capability for controlling the regioselectivity of the process. In this context, the photochemical [2 + 2] cycloaddition reaction of cyclic α,β-unsaturated carbonyl compounds (enones) to alkenes has been studied, both experimentally and theoretically, to gain insight into the regioselectivity. This photochemical reaction is probably the most widely used in synthetic organic chemistry for the synthesis of cyclobutane derivatives.[1] The studies performed previously on this reaction have mainly been focused on the mechanistic aspects that control the regioselectivity, and it was concluded that the initial step of this reaction involves the attack of the triplet $\pi\pi^*$ excited state of the α,β-unsaturated carbonyl compound on the alkene in its ground state, from which a 1,4-biradical intermediate is formed that can evolve through two reactive channels. One is toward ring closure and the formation of the cyclobutane derivative, whereas the other path goes back to the ground-state reagents through retrocleavage. Both pathways proceed via an intersystem crossing.

The regiochemistry observed in this type of reaction has long been of interest. Both regioisomers of the cyclobutane adducts, head-to-head (**HH**) and head-to-tail (**HT**), are obtained as products when the triplet α,β-unsaturated carbonyl compound reacts with electron-rich or electron-deficient olefinic substrates as displayed in Scheme 1. It has been shown experimentally that the isomer ratio depends on the substituent's electronic character: electron-rich alkenes preferentially yield the **HT** isomer, whereas electron-poor alkenes selectively yield the **HH** regioisomer.

In the 1960s, Corey et al.[2] and Eaton[3] first investigated the regioselectivity of the photochemical cycloaddition displayed in Scheme 1. To explain the regioselectivity, Corey et al.[2] proposed the formation of an oriented π complex, or the so-called exciplex model, prior to the formation of a 1,4-biradical intermediate as the controlling agent of the regioselectivity; its orientation was explained in terms of the charge distribution associated with the triplet $n\pi^*$ excited state of the unsaturated ketone, which was proposed as the reactive state for this photochemical reaction. Although this model explains the regioselectivity, it is not supported by experimental evidence because the reactive triplet excited-state enone was found to be $\pi\pi^*$ instead of $n\pi^*$ and the π complex was not detected. Some decades later, Weedon and co-workers[4,5] reported studies based on radical-trapping experiments on the triplet 1,4-biradical intermediate, and they suggested that the **HH/HT** ratio of the biradical intermediate is not fully translated in the cyclobutane adducts ratio because the cyclization process of the biradical competes with the fragmentation process back toward the reactants.

On the other hand, quantum chemical calculations[6−12] have also been carried out on this type of reaction, mainly focusing on investigating the potential energy surface (PES), localizing transition structures, and exploring reaction paths. Other authors have adopted a conceptual standpoint to gain insight into the photochemical reaction and its regioselectivity. Broeker and co-workers[6] performed an unrestricted Hartree−Fock study combined with Møller−Plesset calculations, using acrolein to model the unsaturated carbonyl compound. They found a twisted conformation for the lowest triplet $\pi\pi^*$ excited state of this molecule. Moreover, they also calculated the activation energy barriers for bond formation at the α- and β-carbon atoms using some substituted ethylenes with electron-donating and electron-withdrawing groups. These authors concluded that the biradical formation step governs the regioselectivity. Another study on this reaction was carried out by Wilsey and collaborators,[8] who explored the complete reaction path for the cycloaddition of acrolein to ethylene on both the triplet excited-state and singlet

* To whom correspondence should be addressed. E-mail: pjaqueol@vub.ac.be (P.J.), fdeprof@vub.ac.be (F.D.P.).
† Vrije Universiteit Brussel (VUB).
‡ Pontificia Universidad Católica de Chile.

10.1021/jp807754f CCC: $40.75
Published on Web 12/12/2008

SCHEME 1

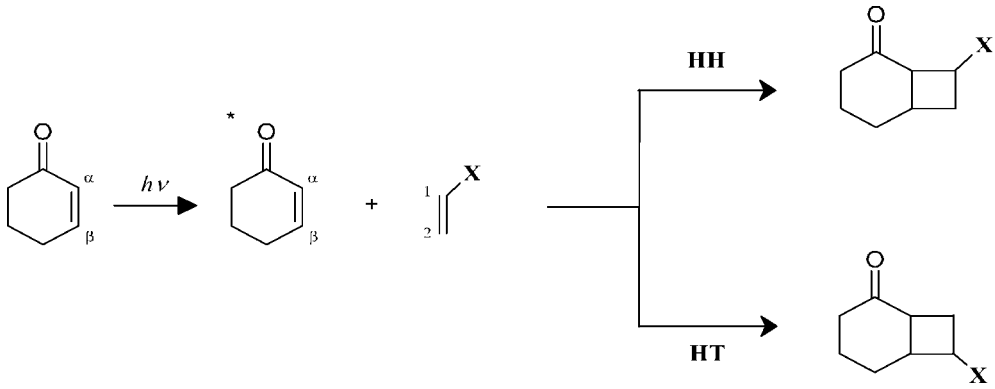

ground-state Born−Oppenheimer potential energy surfaces at the CASSCF level of theory. This study showed that both potential energy surfaces play a key role in determining the regioproduct ratio, as was previously pointed out by Weedon et al.[4,5] For the same model system, Bertrand et al.[9] also carried out a study of the complete reaction path using different computational strategies (among other DFT methods), providing guidelines about the electronic structure methods that are appropriate to describe the different steps that take place in this type of photochemical cycloaddition.

From a different perspective, De Proft et al.[12] studied the regioselectivity in the [2 + 2] photocycloaddition of unsaturated ketones to substituted alkenes from a conceptual density functional theory (DFT)[13−16] point of view. These authors compared the performance of both spin-restricted and spin-polarized DFT-based reactivity descriptors in the prediction of **HH** and **HT** regioisomers. Their analysis focused on the initial response of the reagents in the cycloaddition reaction, which were individually evaluated on the triplet state of enones, using acrolein and α,β-cyclohexenone as model systems and substituted alkenes in their singlet ground states. The supermolecule approach for some reaction pathways was not considered in that study. The local softness in connection with a local version of the hard and soft acids and bases (HSAB) principle was found to explain the regioselectivity expected only when the triplet enone attacks electron-rich alkenes, i.e., when the bond formation is between the β-carbon atom on the carbonyl compound and a substituted carbon atom on the olefin (see Scheme 1). Within a conceptual spin-polarized DFT (SP-DFT) framework, the regioselectivity could be understood through the ad hoc designed local version of the spin philicity and spin donicity concepts, introduced by Pérez et al.,[17] as the interaction between the site on alkenes with highest spin philicity (i.e., the lowest destabilization upon increase of the spin number N_S) with the site presenting the highest change in spin number with decreasing global multiplicity of the unsaturated carbonyl compound.

The conceptual spin-polarized DFT framework,[18] with the electron density and spin density as basic and independent carriers of information, provides a complete hierarchy of electronic chemical reactivity descriptors that have allowed for the rationalization of phenomena such as the forbidden singlet−triplet transition of halocarbenes[19] and the charge redistribution associated with electronic states of different spin multiplicities[20] in its earlier applications. Recently, the SP-DFT chemical descriptors have been successfully applied in the rationalization of types of reactions (cycloaddition,[17] hydrogenation,[21] cyclization[22]), as well as in the prediction of spin properties of different reactive intermediates (carbenes, silylenes, germylenes, stannylenes, nitrines, and phosphinidenes).[23−27] On the other hand, an article published by Pérez et al.[28] provides a mathematical framework for a new spin-resolved representation in SP-DFT.

In general, the conceptual DFT-defined chemical responses that have proven to be powerful interpretative tools for rationalizing the thermodynamic driving force and kinetic aspects associated with a variety of organic and inorganic reactions in both ground and excited states.[14−16] On the other hand, the evolution of DFT response functions along the reaction coordinate ξ[29−33] has also proven to be useful in the identification of the specific interactions that might be operating and controlling the course of a chemical transformation, which is highly relevant from a mechanistic point of view.

A complementary tool for characterizing the reaction mechanisms is the reaction force [$F(\xi)$] concept that was proposed by Toro-Labbé and collaborators.[30,31,34−42] It is a global quantity that depends only on the reaction coordinate, and it is obtained by numerical differentiation of the energy profile with respect to ξ. $F(\xi)$ allows for the definition of three distinct regions along the reaction pathway: reactant, transition state, and product. The significance of the reaction force concept was investigated and presented in a series of articles,[30,31,34−42] where the reaction force profile and the structural and electronic reordering along ξ are considered as a set of key properties providing insight into both the reaction mechanism and the nature of the energy barriers that drive some intramolecular and intermolecular rearrangements.

The aim of the present article is to explore the [2 + 2] photocycloaddition reaction from a combined, complementary analysis through the reaction force concept and conceptual spin-polarized density functional theory, in order to gain new insight into the mechanism of the reaction and the origin of its regioselectivity. This study was carried out considering acrolein, as a model of an α,β-unsaturated carbonyl compound, reacting with ethylene, methoxyethylene, and acrylonitrile. The last two olefins were used to model electron-rich and electron-poor alkenes, respectively. In our approach, we focused on the mechanism of the first step of the photocycloaddition reaction, i.e., the formation of the 1,4-biradical intermediate, because it plays a key role in the regioisomer ratio,[6] as well as a characterization of this system to undergo an intersystem crossing and cyclization, which is based on the SP-DFT response functions after the formation of the biradical.

2. Theoretical Background

2.1. SP-DFT-Based Reactivity Descriptors. Conceptual DFT has rigorously introduced a set of response functions for atomic and molecular systems that have allowed many chemical processes to be described and understood.[13−15] Thereby, theoretical support was provided for previously defined chemical concepts such as electronegativity (χ), which

was identified with the negative of electronic chemical potential [$\chi = -\mu = -(\partial E/\partial N)_{v(\vec{r})}$],[43] and chemical hardness [$\eta = (\partial^2 E/\partial N^2)_{v(\vec{r})}$] and softness ($S = 1/\eta$).[44] Here, E denotes the system's electronic energy, N is the number of electrons, and $v(\vec{r})$ is the external potential (i.e., the potential due to the nuclei for an isolated system). The initial formulation was given for systems without explicit consideration of the spin polarization, with associated spin number N_S. N_S is defined as the difference between the numbers of spin-up ($N_\uparrow$) and spin-down ($N_\downarrow$) electrons: $N_S = N_\uparrow - N_\downarrow$. Afterward, conceptual DFT was extended to include spin-polarization effects, which is important for cases in which $N_\uparrow$ and $N_\downarrow$ differ. This representation affords the theoretical treatment of chemical reactivity with a constrained analysis of the charge-transfer and spin-polarization processes.[45] In the following paragraphs, the spin-related reactivity indices are briefly introduced.

Within the conceptual SP-DFT theoretical framework, both the charge, $\rho(\vec{r}) = \rho_\uparrow(\vec{r}) + \rho_\downarrow(\vec{r})$, and spin, $\rho_S(\vec{r}) = \rho_\uparrow(\vec{r}) - \rho_\downarrow(\vec{r})$, densities are taken as basic and independent variables. Two Lagrange multipliers, μ_N and μ_S, are obtained from a minimization procedure of the energy functional under the normalization constraints $\int \rho(\vec{r})\, d\vec{r} = N_\uparrow + N_\downarrow = N$ and $\int \rho_S(\vec{r})\, d\vec{r} = N_\uparrow - N_\downarrow = N_S$. They are identified as constrained chemical (μ_N) and spin (μ_S) potentials. For an N-electron system with spin number N_S at external potential $v(\vec{r})$ and external magnetic field $B(\vec{r})$, μ_N and μ_S are given by the following first derivatives

$$\mu_N = \left(\frac{\partial E}{\partial N}\right)_{N_S, v(\vec{r}), B(\vec{r})} \tag{1}$$

and

$$\mu_S = \left(\frac{\partial E}{\partial N_S}\right)_{N, v(\vec{r}), B(\vec{r})} \tag{2}$$

The generalized potentials are global properties that allow for the characterization of the chemical systems as a whole. μ_N carries information comparable to that of the electronic chemical potential in spin-restricted DFT:[43] it measures the tendency to undergo charge transfer, except that it is estimated at constant N_S. The spin potential provides a measure for the tendency of a system to change its spin polarization when N is kept fixed. In the SP-DFT case, the left-hand (−) and right-hand (+) derivatives are different because of the discontinuities in both N and N_S. $\mu_N^{(m)}$ ($m = -, +$) maintains the same definition for charge-transfer processes as in the spin-restricted theory, except that equal amounts of spin-up and spin-down electrons are removed or attached. $\mu_S^{(-)}$ describes changes in the direction of decreasing N_S, and $\mu_S^{(+)}$ describes changes in the direction of increasing N_S, both at fixed N. These descriptors can provide an understanding about both radiative (e.g., phosphorescence) and radiationless (e.g., intersystem crossing) nonadiabatic transitions of an electronically excited system such as those studied in the present work.

Other global charge- and spin-related reactivity descriptors are the so-called generalized hardnesses, which, in the $E = E[N, N_S, v(\vec{r}), B(\vec{r})]$ representation, are defined as

$$\eta_{NN} = \left(\frac{\partial \mu_N}{\partial N}\right)_{N_S, v(\vec{r}), B(\vec{r})} = \left(\frac{\partial^2 E}{\partial N^2}\right)_{N_S, v(\vec{r}), B(\vec{r})}$$

$$\eta_{NS} = \left(\frac{\partial \mu_N}{\partial N_S}\right)_{N, v(\vec{r}), B(\vec{r})} = \left(\frac{\partial \mu_S}{\partial N}\right)_{N_S, v(\vec{r}), B(\vec{r})} = \eta_{SN} \tag{3}$$

$$\eta_{SS} = \left(\frac{\partial \mu_S}{\partial N_S}\right)_{N, v(\vec{r}), B(\vec{r})} = \left(\frac{\partial^2 E}{\partial {N_S}^2}\right)_{N, v(\vec{r}), B(\vec{r})}$$

As for spin-restricted DFT,[44] η_{NN} corresponds to the curvature of the $E = E(N)_{N_S, v(\vec{r}), B(\vec{r})}$ function and it measures the resistance to charge transfer when the spin number is kept fixed. η_{NS} and η_{SN} can be seen as cross-terms which provide additional information and η_{SS} has been called the spin hardness, and measures the curvature of the $E = E(N_S)_{N, v(\vec{r}), B(\vec{r})}$ function.

Extending the procedure proposed by Parr et al.[46] to define the electrophilicity index, $\omega = \mu^2/2\eta$, to the spin-polarized DFT yields philicity concepts for constrained charge-transfer (ω_N) and spin-polarization ($\omega_S^\pm$) processes[45]

$$\omega_N = \frac{(\mu_N)^2}{2\eta_{NN}} \tag{4}$$

and

$$\omega_S^\pm = \frac{(\mu_S^\pm)^2}{2\eta_{SS}} \tag{5}$$

ω_N is a constrained electrophilicity index, measuring the capability of a systems to acquire optimal electronic charge at fixed spin number.

Equation 5 defines the philicity index, $\omega_S^\pm$, for a spin-polarization process. It has been called spin-philicity and spin-donicity, respectively, when the change in spin number, ΔN_S, is positive (+) and negative (−) (i.e., when the spin number is increasing and decreasing, respectively) and has been proposed as a measure of the capability of a system to change its spin polarization in the absence of electron transfer.

The set of reactivity indices described allows for the characterization of the system's reactivity as a whole, whereas the local information is carried by the Fukui function [$f(\vec{r})$]. In spin-restricted theory, this function was introduced by Parr and Yang as[47]

$$f(\vec{r}) = \left(\frac{\delta \mu}{\delta v(\vec{r})}\right)_N = \left(\frac{\partial \rho(\vec{r})}{\partial N}\right)_{v(\vec{r})} \tag{6}$$

Because of the discontinuity of this derivative at integer N, three Fukui functions are defined governing nucleophilic [$f^+(\vec{r})$], electrophilic [$f^-(\vec{r})$], and radical [$f^0(\vec{r})$] attacks. These functions can be condensed on atoms or functional groups. In this context, a simple scheme based on the frozen-core approximation was proposed by Contreras et al.,[48] in which these indices can be computed from the densities of the frontier molecular orbitals, i.e., the highest occupied molecular orbital (HOMO) or lowest unoccupied molecular orbital (LUMO):[49] $f^+(\vec{r}) \approx \rho_{LUMO}(\vec{r})$, $f^-(\vec{r}) \approx \rho_{HOMO}(\vec{r})$, and $f^0(\vec{r}) \approx [f^+(\vec{r}) + f^-(\vec{r})]/2$. As the frontier molecular orbitals are typically expanded into an atomic basis set, the Fukui index can be condensed to atomic region k as[48]

$$f_k^\alpha = \sum_{\mu \in k} \sum_\nu C_{\mu\alpha} C_{\nu\alpha} S_{\mu\nu} \tag{7}$$

where $S_{\mu\nu}$ is an element of the overlap matrix and $\{C_{\mu\alpha}, C_{\nu\alpha}\}$ are the expansion coefficients of the frontier molecular orbital, α = HOMO or LUMO, to obtain the condensed Fukui indices at site k, f_k^- and f_k^+, respectively.

TABLE 1: Reaction Energy (ΔE°) and Energy Barrier ($\Delta E^\ddagger$) Computed at the B3LYP/6-311+G(d,p) Level for Both α- and β-Attack Reaction Paths (RPs) of the Reaction between $^3\pi\pi^*$ Acrolein and Ethylene[a]

RP	ΔE°	$\Delta E^\ddagger$
	α Attack	
a	−8.82	10.58
b	−8.55	9.84
c	−7.94	10.33
average	−8.44	10.25
SD	0.45	0.38
	β Attack	
d	−22.21	6.68
e	−20.80	7.46
f	−20.34	7.57
average	−21.12	7.24
SD	0.97	0.49

[a] All values in kcal/mol.

Within the more general spin-polarized DFT $E = E[N,N_S,v(\vec{r}),B(\vec{r})]$ representation, the so-called generalized Fukui functions[18] are obtained, which are written as

$$f_{NN}(\vec{r}) = \left(\frac{\partial \rho(\vec{r})}{\partial N}\right)_{N_S,v(\vec{r}),B(\vec{r})} = \left(\frac{\delta \mu_N}{\delta v(\vec{r})}\right)_{N,N_S,B(\vec{r})}$$

$$f_{SN}(\vec{r}) = \left(\frac{\partial \rho_S(\vec{r})}{\partial N}\right)_{N_S,v(\vec{r}),B(\vec{r})} = -\frac{1}{\mu_B}\left(\frac{\delta \mu_N}{\delta B(\vec{r})}\right)_{N,N_S,v(\vec{r})}$$

$$f_{NS}(\vec{r}) = \left(\frac{\partial \rho(\vec{r})}{\partial N_S}\right)_{N,v(\vec{r}),B(\vec{r})} = \left(\frac{\delta \mu_S}{\delta v(\vec{r})}\right)_{N,N_S,B(\vec{r})} \quad (8)$$

$$f_{SS}(\vec{r}) = \left(\frac{\partial \rho_S(\vec{r})}{\partial N_S}\right)_{N,v(\vec{r}),B(\vec{r})} = -\frac{1}{\mu_B}\left(\frac{\delta \mu_S}{\delta B(\vec{r})}\right)_{N,N_S,v(\vec{r})'}$$

where μ_B is the electron Bohr magneton. These functions are defined as variations of the generalized chemical (μ_N) and spin (μ_S) potentials with respect to external or magnetic potentials, when N and N_S are kept fixed. These functional derivatives can also be written as responses of the electron charge density, $\rho(\vec{r})$, and spin density, $\rho_S(\vec{r})$, to a change in N or N_S through Maxwell relations. Also, condensation to a region k was recently proposed by Chamorro and Pérez within the SP-DFT framework,[50] which corresponds to an extension of the scheme outlined earlier.

In the present study, we use the global responses and some of these generalized Fukui indices to characterize the biradical intermediate formed upon attack of triplet $\pi\pi^*$ acrolein to alkenes in their ground state. In this sense, the concept of spin donicity, ω_S^-, provides information about the capability of the system to change its spin multiplicity, whereas $f_{NS,k}^-$ and $f_{SS,k}^-$ provide information about the electron and spin density reorganization, respectively, taking place when the biradical intermediate undergoes an intersystem crossing from the triplet PES to the singlet PES, i.e., when N_S decreases at constant N.

2.2. Energy and Force Profiles. Within the Born−Oppenheimer[51] potential energy surface, it is possible to describe a chemical reaction through the changes of the molecular geometry in a $(3M - 6)$-dimensional space for a nonlinear systems with M atoms, by the intrinsic reaction coordinate (IRC) model proposed by Fukui.[52] Some of the present authors have defined the reaction force concept, $F(\xi)$, which is given by numerical differentiation of the energy profile

$$F(\xi) = -\frac{dE}{d\xi} \quad (9)$$

$F(\xi)$ is zero for every stationary point [reactant (R), transition state (TS), and product (P)], negative in the regions defined from the reactant to the transition state, and positive in the region defined from TS to P, passing through minimum and maximum values at the first (ξ_1) and second (ξ_2) inflection points of $E(\xi)$. This pattern allows three regions to be defined for a one-step reaction, namely, reactant, transition state, and product, with well-established tendencies as evidenced in refs 30, 31, and 34− 42. In the reactant region ($\xi_R \le \xi < \xi_1$), a retarding force is observed because the reactive species are prepared or activated through some distortions along of their $(3M - 6)$ internal degrees of freedom (bond stretching, bending, rotations, etc). The transition-state region ($\xi_1 \le \xi < \xi_2$) is governed by the transition to product involving bond-breaking and bond-making processes accompanied by strong fluctuations in some electronic properties (for instance, electronic populations, molecular electrostatic potential, Fukui functions, etc); on the other hand, this produces a positive driving force that is maximal at ξ_2. Finally, the product region ($\xi_2 \le \xi < \xi_P$) is mainly dominated by the relaxation process toward the equilibrium geometry of the product.

Each of these processes along ξ can be characterized by the amount of work, which is given by

$$W_{a\to b} = -\int_a^b F(\xi)\, d\xi \quad (10)$$

Within this scheme, the energy barrier, $\Delta E^\ddagger$, can be written as the sum of two contributions

$$\Delta E^\ddagger = -\int_{\xi_R}^{\xi_1} F(\xi)\, d\xi - \int_{\xi_1}^{\xi_{TS}} F(\xi)\, d\xi = W_{\xi_R\to\xi_1} + W_{\xi_1\to\xi_{TS}} \quad (11)$$

This partitioning proved to be valuable for elucidating the solvent and catalyst effects on specific reactions due to the fact that the first term is associated with structural effects whereas the electronic factors are associated with the second term of eq 11.[39,41,42]

3. Computational Details

For the addition of acrolein to olefins, all geometry optimizations of the transition states on the triplet excited-state potential energy surface were performed using the hybrid exchange-correlation functional B3LYP[53,54] under an unrestricted scheme together with the standard 6-311+G(d,p)[55,56] basis set in the Gaussian 03 program.[57] This exchange-correlation functional was chosen following the study published by Bertrand et al.[9] where it produced energy values, such as ΔE° and $\Delta E^\ddagger$, for the 1,4-biradical intermediate formation step that were comparable to those obtained by the coupled-cluster method. The minimum-energy paths were obtained through the intrinsic reaction coordinate (IRC) procedure[52,58] using a gradient step size of 0.10 amu$^{1/2}$ bohr. We also performed harmonic vibrational frequency analysis to confirm that the transition structures are first-order saddle points whereas the reactants and products correspond to minima on the potential energy surfaces for the three reactions studied, in both the **HH** (or β) and **HT** (or α) pathways, displayed in Figure 1.

The global and local spin-polarized reactivity indices can be estimated through the following working equations, which are based on the well-known finite difference and frozen core approximations. The expressions used to estimate $\mu_S^{(-)}$ and $\mu_S^{(+)}$ are written in terms of the HOMO and LUMO eigenvalues of both spin symmetries, up (↑) and down (↓)

$$\mu_S^{(-)} \approx \frac{1}{2}(\varepsilon_{HOMO}^{\uparrow} - \varepsilon_{LUMO}^{\downarrow})$$
$$\mu_S^{(+)} \approx \frac{1}{2}(\varepsilon_{LUMO}^{\uparrow} - \varepsilon_{HOMO}^{\downarrow}) \quad (12)$$

The spin hardness, η_{SS}, associated with a change in spin multiplicity from the triplet (t) to the singlet (s) potential energy surface, as in the present case, is given by

$$\eta_{SS}^{t\rightarrow s} \approx \frac{\mu_S^{(+)s} - \mu_S^{(-)t}}{\Delta N_S} \quad (13)$$

where $\mu_S^{(+)s}$ is the spin potential of the singlet in the direction of increasing N_S and $\mu_S^{(-)t}$ is the spin potential of the triplet state in the direction of decreasing N_S. As the reference in our case, the triplet potential energy surface, $\mu_S^{(+)s}$, is evaluated at the triplet-state geometry generated by the IRC, with $\Delta N_S = -2$.

The generalized Fukui indices that have been condensed to atoms can be calculated from the HOMO and LUMO spin-shape factors [$\sigma^{i,j}(\vec{r}) \equiv |\phi^{i,j}(\vec{r})|^2$ for i = HOMO, LUMO and $j = \uparrow, \downarrow$], as was pointed out by Galván and collaborators[18] and implemented by Chamorro and Pérez.[50] The Fukui indices used by us, $f_{NN,k}^{\pm 0}$, $f_{NS,k}^{-}$, and $f_{SS,k}^{-}$, are given by the following expressions

$$f_{NN,k}^{-} \approx \frac{1}{2}(\sigma_k^{HOMO,\uparrow} + \sigma_k^{HOMO,\downarrow})$$
$$f_{NN,k}^{+} \approx \frac{1}{2}(\sigma_k^{LUMO,\uparrow} + \sigma_k^{LUMO,\downarrow}) \quad (14)$$
$$f_{NN,k}^{0} = \frac{1}{2}(f_{NN,k}^{-} + f_{NN,k}^{+})$$
$$f_{NS,k}^{-} \approx \frac{1}{2}(\sigma_k^{HOMO,\uparrow} - \sigma_k^{LUMO,\downarrow}) \quad (15)$$

and

$$f_{SS,k}^{-} \approx \frac{1}{2}(\sigma_k^{HOMO,\uparrow} + \sigma_k^{LUMO,\downarrow}) \quad (16)$$

The spin-shape factors were estimated by the same procedure as implemented for $f_k^{\pm}$ in spin-nonpolarized theory as indicated by eq 7, taking into account the degeneracy of the frontier molecular orbital for each spin symmetry.

The data for computing the above-mentioned DFT-based reactivity descriptors were obtained through single-point calculations at the B3LYP/6-311G(d,p)[55] level of theory for the 1,4-biradical intermediate determined by the IRC scheme with the 6-311+G(d,p) basis set.

We also tested the stability[59,60] of the B3LYP/6-311G(d,p) wave function of the biradical intermediates. In the triplet state, all wave functions were found to be stable. However, those obtained in the singlet state at the same triplet-state geometries are usually not stable mainly because of restricted and unrestricted instabilities. Consequently, the wave function on the singlet surface was always allowed to become unrestricted.

4. Results and Discussion

In a first part, the results of the triplet excited-state PES for the addition of acrolein to ethylene (**R1**) are presented. Following the work by Wilsey et al.,[8] we optimized the geometries of the transition states where three conformations for each type of attack (by α- and β-carbon atoms) were found, as displayed in Figure 2; every structure is indicated using the same nomenclature as in ref 8. The geometries obtained at the B3LYP/6-311+G(d,p) level are close to those reported previously, in which case the CASSCF/6-31G(d) method was used. The reaction energies ($\Delta E°$) and energy barriers ($\Delta E^{\ddagger}$) for both attacks are summarized in Table 1. The data do not show a significant preference among the three paths for each type of attack, as can be noticed by the average and standard deviation values, also included in Table 1. Note that the 1,4-biradical intermediate formed through the β-attack path is thermodynamically more stable, by about 12−13 kcal/mol, than that formed by the α pathway. This preference arises from the delocalization of the radical center on the α-carbon atom over the carbonyl group, as was pointed out by Erickson and Kahn.[61] Furthermore, the β attack is also the kinetically preferred path, by approximately 3 kcal/mol. This result is in agreement with the CASSCF calculations of Wilsey et al.,[8] and it is considerably larger than the preference predicted by PMP3/6-31G(d)//UHF/3-21G calculations performed by Broeker et al.,[6] who computed a difference of only 0.3 kcal/mol.

For reactions with electron-rich (**R2**) and electron-poor (**R3**) alkenes, we located all possible conformations of the transition states for the addition of triplet excited-state acrolein to substituted olefins with electron-donating (methoxy, —OMe) and electron-withdrawing (cyano, —CN) groups. The stationary points for the most-favorable reactive channel for each type of attack are depicted in Figure 1. Here, we note that the biradical intermediate presents a gauche-out conformation for **R1** and **R3** and an anti conformation for **R2** when it is reached by an α-attack mechanism, whereas it presents a gauche-anti conformation when it is formed through a β-attack mechanism for **R1**−**R3**.

Surprisingly, as can be noted from Figure 1, in both cases, the α- or β-carbon atom of acrolein attacks the alkene on the least-substituted carbon atom; on the other hand, the α attack generates an intermediate that could yield the **HT** regioisomer as the cycloadduct, whereas the **HH** regioproduct could be formed through the β-attack mechanism. The energetic properties, $\Delta E°$ and $\Delta E^{\ddagger}$, associated with the two reactive channels are reported in Table 2, where we have included the values with the lowest energy barrier from Table 1 to characterize **R1** (paths b and d for the α and β attacks, respectively). They are compared with the data for **R2** and **R3**. Again, our results on the addition of acrolein to electron-rich and electron-poor olefins show that the most-favorable pathway, both thermodynamically and kinetically, is the β attack, predicting the same regioproduct for both reactions with substituted alkenes, i.e., the formation of the **HH** isomer, which apparently contradicts the expected regioselectivity, for example, from the theoretical study reported by Broeker et al.[6] However, when acrolein reacts with methoxyethylene, the energy barrier differences between the two kinds of attacks, $\Delta\Delta E^{\ddagger} = \Delta E^{\ddagger}(\alpha) - \Delta E^{\ddagger}(\beta)$, is only 0.9 kcal/mol in favor of the β path, whereas it is 3.16 and 4.18 kcal/mol for **R1** and **R3**, respectively.

To gain insight into this finding, a detailed analysis of the potential energy, reaction force, and spin-polarized density-functional-theory-based reactivity descriptors was carried out for both types of attack for the three reactions.

4.1. Energy and Reaction Force. The minimum-energy paths and reaction force associated with the formation of the 1,4-biradical intermediate, for the addition of the triplet $\pi\pi^*$ excited-state acrolein to ethylene and substituted olefins through α and β attack, are displayed in Figures 3 and 4, respectively. A substituent effect on both pathways can be observed when the thermodynamic data, reported in Table 2, are compared with those for the reaction with ethylene (**R1**). Electron-donating and electron-withdrawing groups stabilize the biradical intermediate, by 2.19 and 6.09 kcal/

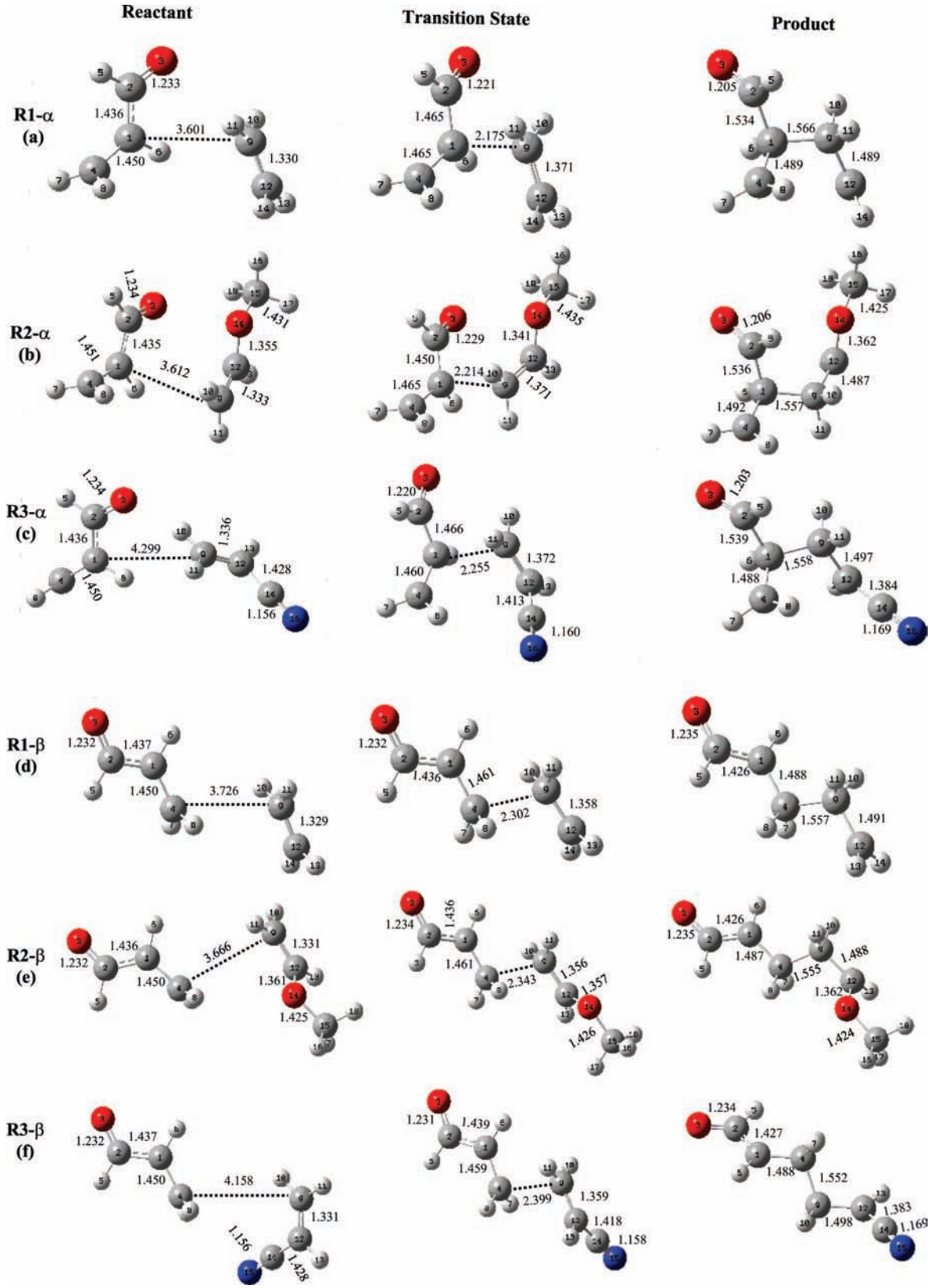

Figure 1. Stationary structures determined at the B3LYP/6-311+G(d,p) level of theory for the 1,4-biradical intermediate formation step through the (a−c) α and (d−f) β pathways for the [2 + 2] photocycloaddition reaction between the $^3\pi\pi^*$ excited state of acrolein and (**R1**) ethylene, (**R2**) methoxyethylene, and (**R3**) acrylonitrile.

mol, respectively, when the reaction follows an α pathway, whereas it is stabilized by 2.91 and 7.44 kcal/mol, respectively, for a β-attack mechanism. The effect is also observed on the energy barrier, which decreases when acrolein reacts with substituted olefins in both pathways. The reaction with the electron-rich alkene (X = −OMe) is faster than that with the electron-poor alkene (X = −CN) by an α-attack mechanism whereas the reverse situation is obtained for the β pathway, except that the energy barrier ($\Delta E^{\ddagger}$) for the elec-

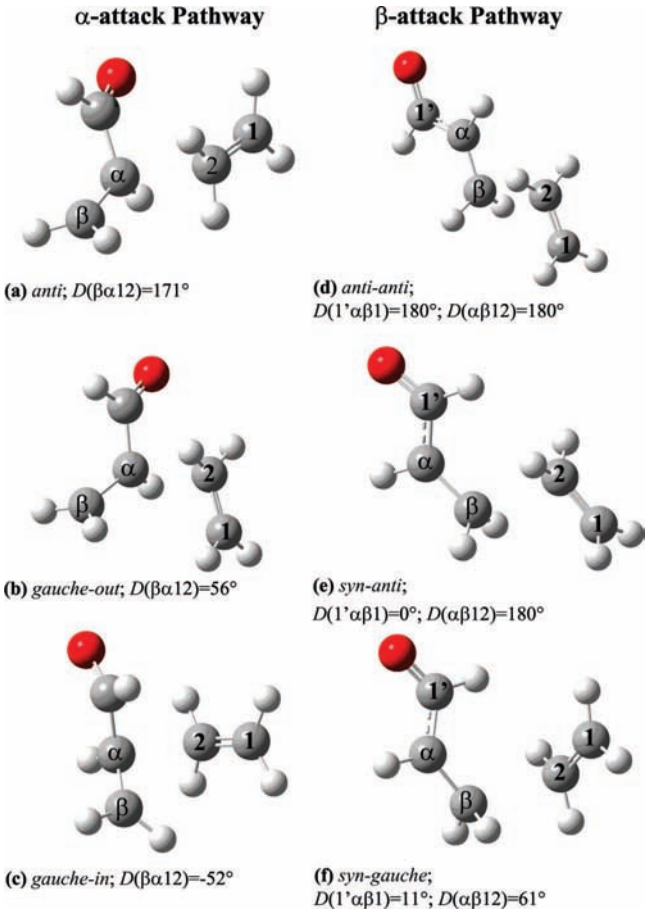

Figure 2. Transition structures found for the 1,4-biradical intermediate formation step from the reaction between $^3\pi\pi^*$ excited-state acrolein and ethylene at the B3LYP/6-311+G(d,p) level of theory: (a−c) α- and (d−f) β-attack pathways.

TABLE 2: Reaction Energy (ΔE°), Energy Barrier ($\Delta E^\ddagger$), and Amount of Work ($W_{a\to b}$) Computed at the B3LYP/6-311+G(d,p) Level for the Formation of the 1,4-Biradical Intermediates from the Addition of $^3\pi\pi^*$ Acrolein to Olefins through Both the α and β Pathways[a]

	ΔE°	$\Delta E^\ddagger$	$W_{\xi_R\to\xi_1}$	$W_{\xi_1\to\xi_{TS}}$	$-W_{\xi_{TS}\to\xi_2}$	$-W_{\xi_2\to\xi_P}$
			α Path			
R1	−8.55	9.84	7.11	2.73	8.36	10.03
R2	−10.74	6.48	4.64	1.84	9.01	8.21
R3	−14.64	9.14	6.85	2.29	10.44	13.35
			β Path			
R1	−22.21	6.68	4.75	1.93	13.75	15.14
R2	−25.12	5.58	3.38	2.20	16.31	14.39
R3	−29.65	4.96	3.34	1.62	15.07	19.54

[a] All values in kcal/mol.

tron-poor alkene is slightly lower than that for the reaction with electron-rich alkene.

The amount of work ($W_{a\to b}$) involved at each step along ξ was obtained by integration of the reaction force profile as indicated by eq 10. These values are also quoted in Table 2 for both paths of reactions **R1**−**R3**. In previous investigations, we showed that the first step of an elementary process is associated with the structural reorganization of the reactants in an activated reactant configuration, reached at ξ_1.[31,34−36,41,42] In the present situation, the corresponding amount of work basically involves bringing the α,β-enone and the alkene closer to each other. Note that, for each reaction, the $W_{\xi_R\to\xi_1}$ values for the α path are higher than those for the β path, possibly because of steric effects, as

TABLE 3: Global Spin-Related Reactivity Descriptors of the 1,4-Biradical Intermediate Formed through the α (or HT) and β (or HH) Pathways at the B3LYP/6-311G(d,p) Level[a]

	$\mu_S^{(-)t}$	$\mu_S^{(+)s}$	$\eta_{SS}^{t\to s}$	ω_S^-
		α Path		
R1	−1.71	1.82	−1.77	−0.83
R2	−1.18	1.81	−1.49	−0.47
R3	−1.43	1.65	−1.54	−0.66
		β Path		
R1	−1.27	1.65	−1.46	−0.55
R2	−0.73	1.62	−1.13	−0.23
R3	−1.52	1.67	−1.59	−0.72

[a] All values in eV.

TABLE 4: Atom-Condensed SP-DFT Fukui Indices, $f_{NS,k}^-$ and $f_{SS,k}^-$, of the 1,4-Biradical Intermediate Formed through the α and β Pathways for R1−R3[a]

	α path				β path		
	atom k	$f_{NS,k}^-$	$f_{SS,k}^-$		atom k	$f_{NS,k}^-$	$f_{SS,k}^-$
R1	O	0.0050	0.0938	**R1**	O	−0.1316	0.1605
	C_α	0.0320	0.0370		C_α	−0.2330	0.2961
	C_β	−0.2421	0.4513		C_β	0.0203	0.0360
	C_1	0.2421	0.2549		C_1	0.3705	0.3874
	C_2	0.0014	0.0272		C_2	0.0053	0.0206
R2	O	−0.0371	0.0453	**R2**	O	−0.1444	0.1487
	C_α	0.0165	0.0261		C_α	−0.2615	0.2712
	C_β	−0.3260	0.3565		C_β	0.0110	0.0268
	C_1	0.2999	0.3289		C_1	0.3221	0.3285
	C_2	0.0044	0.0153		C_2	0.0035	0.0167
R3	O	0.0679	0.0757	**R3**	O	−0.0875	0.1617
	C_α	0.0073	0.0326		C_α	−0.1488	0.3110
	C_β	0.3115	0.3174		C_β	0.0090	0.0263
	C_1	−0.2905	0.3126		C_1	0.1538	0.2597
	C_2	0.0069	0.0177		C_2	0.0079	0.0222

[a] Values obtained at the B3LYP/6-311G(d,p) level.

can be seen in Figure 1. Furthermore, for both mechanisms, it is observed that the presence of a substituent makes it easier to reach the nuclear configuration at ξ_1, by 2.47 and 0.26 kcal/mol for the α path and by 1.37 and 1.41 kcal/mol for the β path when the alkene is substituted with electron-donating and electron-withdrawing groups, respectively. This is possibly due to electronic effects associated with the substituent, such as inductive and mesomeric effects, helping to bring the reactive species closer to each other to reach the configuration at ξ_1.

The **TS** region has been characterized as one where chemical bonds can be formed and/or broken with or without accompanying nuclear rearrangements. The amount of work involved is given by the zones defined by the minimum and maximum forces passing through **TS** where the retarding and forward forces are equalized. The total amount of work, $W_{\xi_1\to\xi_{TS}} - W_{\xi_{TS}\to\xi_2}$, is made up of one positive term due to a retarding force [$F(\xi) < 0$] and one negative term due to a forward force [$F(\xi) > 0$]. Note that the first term does not present a strong influence for substituted olefins; rather, the forward force is more dependent on the olefinic substrate, the effect being more important for the β pathway (see $-W_{\xi_{TS}\to\xi_2}$ values in Table 2).

It is interesting to analyze the composition of the energy barrier as indicated by eq 11. As has been mentioned, a catalytic effect is observed when substituted olefins are used as the substrate. The contributions to $\Delta E^\ddagger$ are almost constant for the α mechanism (about 72% for $W_{\xi_R\to\xi_1}$ and 28% for $W_{\xi_1\to\xi_{TS}}$), whereas they vary significantly for the β mechanism: **R1**, 71% vs 29%; **R2**, 61% vs 39%; and **R3**, 67% vs 33%. Although the

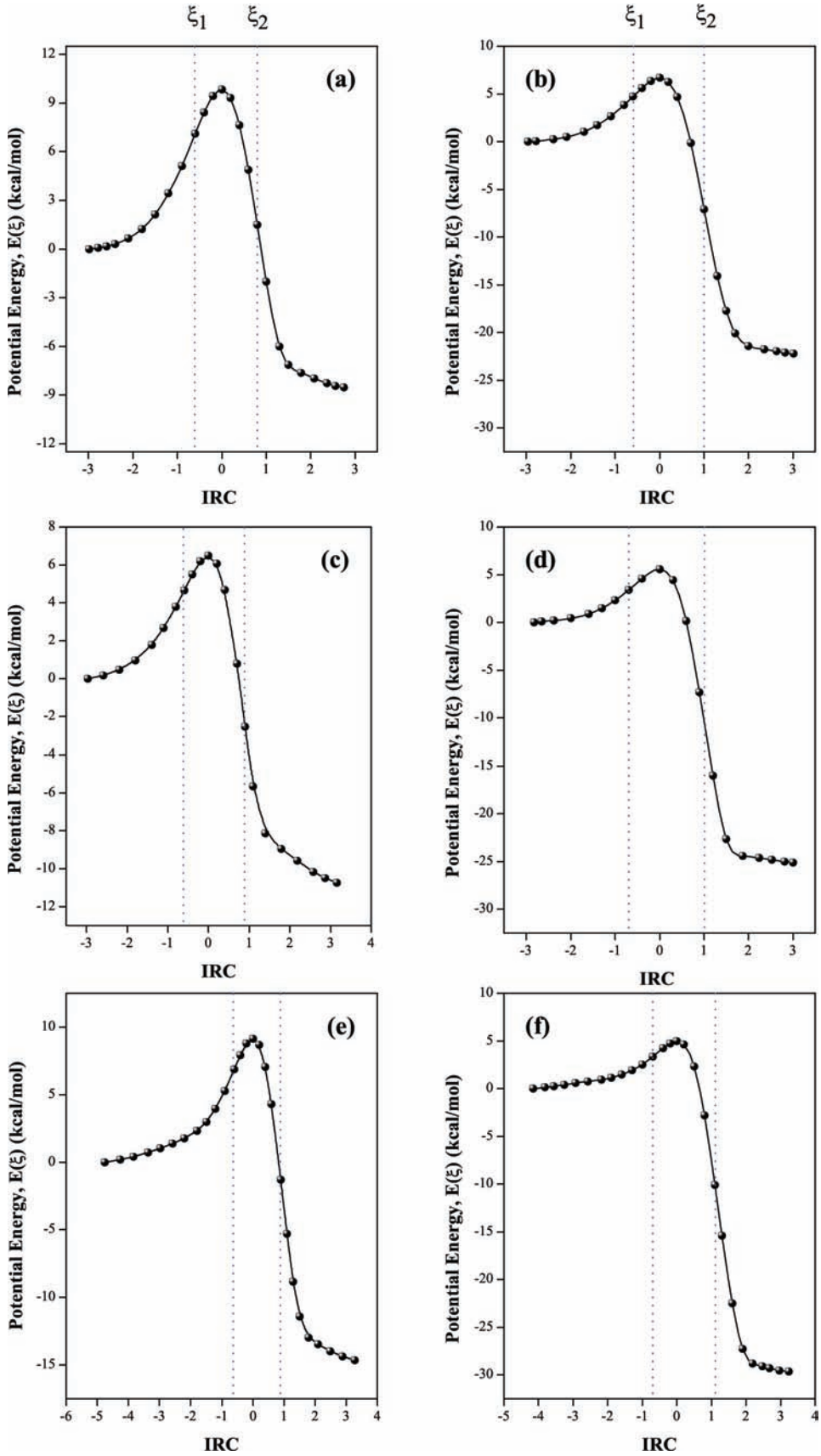

Figure 3. Potential energy profiles associated with (a,c,e) α and (b,d,f) β attacks for the 1,4-biradical intermediate formation step from the reaction between $^3\pi\pi^*$ acrolein and olefins: (a,b) **R1**, (c,d) **R2**, and (e,f) **R3**.

values of $W_{\xi_1 \rightarrow \xi_{TS}}$ are small, we can note that $W_{\xi_1 \rightarrow \xi_{TS}}(\alpha) < W_{\xi_1 \rightarrow \xi_{TS}}(\beta)$ for **R2**, whereas the opposite tendency is observed for **R1** and **R3**. Possibly, this fact is responsible for the formation of the **HT** regioisomer in reactions with electron-rich alkenes.

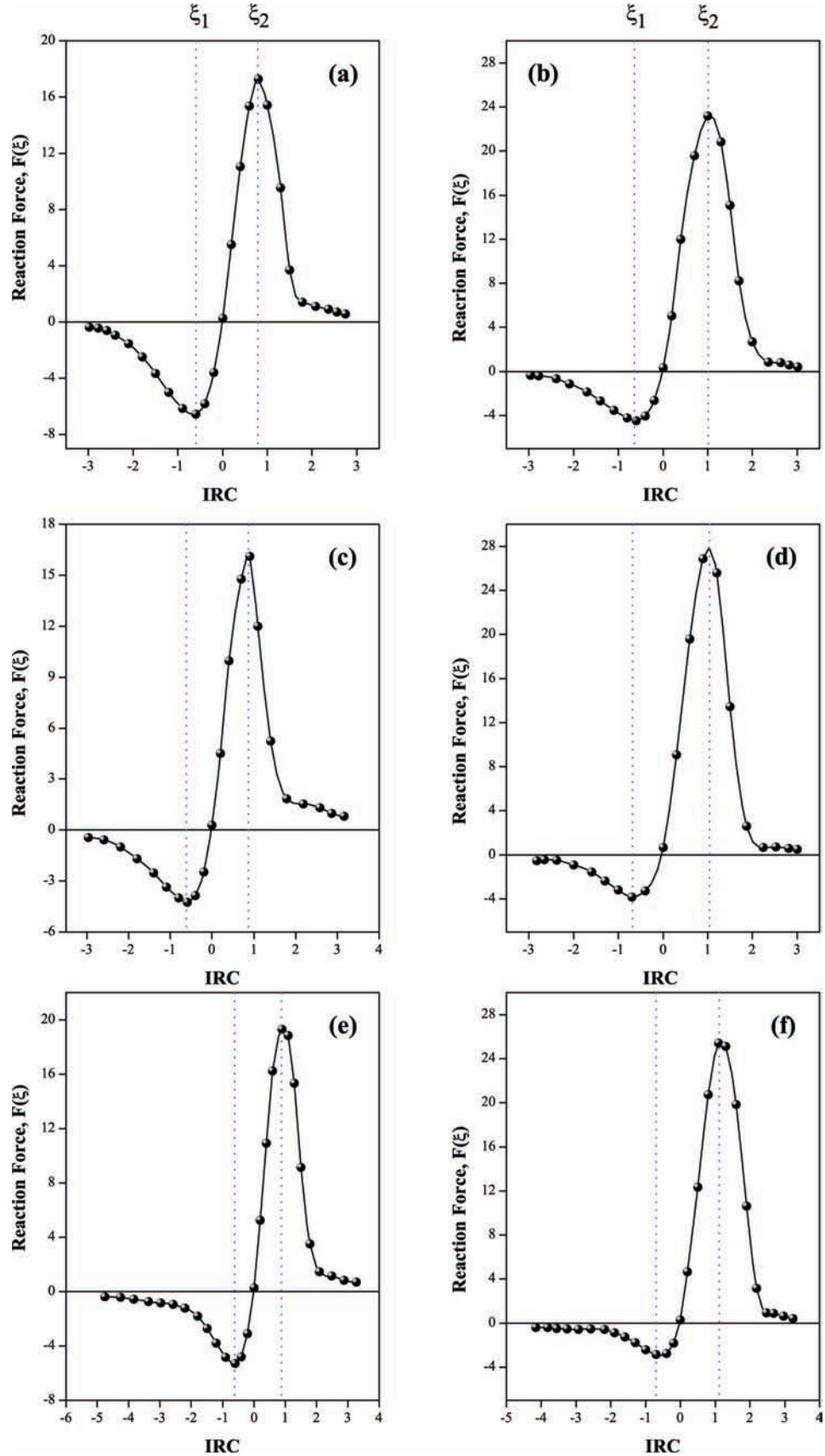

Figure 4. Reaction force profiles associated with (a,c,e) α and (b,d,f) β attacks for the 1,4-biradical formation step from the reaction between $^3\pi\pi^*$ acrolein and olefins: (a,b) **R1**, (c,d) **R2**, and (e,f) **R3**.

Finally, in the product region, the new bonds are relaxed to reach the equilibrium geometry of the biradical intermediate. The amount of work involved in this region for the α path is lower than the relaxation process that takes place when the reaction advances by a β attack (see Table 2). However, the final step shows a substituent effect different to that

previously observed. It is possible to see the electronic character of the substituent because $-W_{\xi_2 \to \xi_P}$ increases in the order methoxyethylene < ethylene < acrylonitrile for both the α- and β-attack mechanisms.

In summary, we have found that the most favorable pathway is when the reaction advances through a β attack, which enables the reactant molecules to approach closer to each other, forming the most stable 1,4-biradical intermediate. Therefore, our results suggest that the **HH** cycloadduct would be formed for the three systems studied. However, for reactions with an electron-rich alkene, the two mechanisms compete because of the small $\Delta\Delta E^{\ddagger}$ values, i.e., the **HT** regioisomer is also expected when this is compared with **R3**, which is more regioselective. As has been mentioned, the fragmentation of the 1,4-biradical intermediate toward reactants in their ground state is another process that could take place. Both of these reaction channels, cyclization and fragmentation, are driven by an intersystem crossing. In this sense, the reaction force, depending only on the Born−Oppenheimer potential energy profile, does not contain information on the capability of the system to cross to another electronic state with a different spin multiplicity. Therefore, an analysis based on spin-related DFT descriptors might be needed to provide this kind of information.

4.2. SP-DFT-Based Reactivity Descriptors. As was emphasized previously, the potential energy and reaction force analysis on the minimum-energy paths for the reaction between the triplet ππ* acrolein to olefins provide information only about the energetics and the mechanism that operate to form the 1,4-biradical intermediate species. From this perspective, however, one cannot predict how it will deactivate or along which pathway it will proceed. Conceptual spin-polarized density functional theory offers an attractive theoretical framework to investigate this issue. The global and local response functions, which measure the initial response of the energy and electron and spin densities in the direction of decreasing spin number, contain valuable information on the intersystem crossing from the triplet to the singlet state. From this analysis, one expects to find the intrinsic capability of the 1,4-biradical intermediate to change its spin multiplicity, as described by the spin donicity ω_S^-. The SP-DFT atom-condensed Fukui indices, $f_{NS,k}^-$ and $f_{SS,k}^-$, provide information about the sites that more susceptible to accumulation and depletion of $\rho(\vec{r})$ and $\rho_S(\vec{r})$, respectively. The $f_{NN,k}^-$, $f_{NN,k}^+$, and $f_{NN,k}^0$ Fukui indices, on the other hand, contain information on the cyclization process of the 1,4-biradical intermediate in the singlet state.

The global spin-related reactivity descriptors associated with the transition from the triplet to the singlet PES of the 1,4-biradical intermediate formed by both mechanisms, α and β attacks, are reported in Table 3. The spin potentials in the cases in which the spin multiplicity is decreasing ($\mu_S^{(-)r}$) and increasing ($\mu_S^{(+)s}$) provide a measure of the tendency of a system to change the spin polarization, whereas spin hardness (η_{SS}^{-s}) can be taken as the curvature of E as a function of N_S. The values given in Table 3 show that the intermediate formed by a β pathway presents a higher tendency to change its spin multiplicity and a lower resistance to produce such a change than that formed by an α pathway, except for the species formed in reactions with electron-poor alkenes (**R3**), for which the two intermediates present comparable spin-related descriptors. The spin-philicity indices, $\omega_S^{\mp}$, have been proposed as philicity for the spin-polarization process. In many cases, for instance, substituted silylenes, nitrenes, and phosphinidenes, the philicity for spin polarization correlates well with the vertical transition energies.[23,24,26] In our case, the spin donicity, ω_S^-, can be taken as a measure of the stabilization when an electronically excited system undergoes an intersystem crossing from the triplet potential energy surface to the singlet PES. As can be seen in Table 3, the intermediates formed by a β mechanism present a higher capability for spin polarization than those formed by an α mechanism, except for the reaction with acrylonitrile, for which the two intermediates present similar values (−0.66 eV for the α path vs −0.72 eV for the β path). It is interesting to note that the intermediates formed in the reaction with methoxyethylene show the highest capability to deactivate the excited state. On the other hand, these intermediates also prove to be more competitive in their formation.

Concerning the local aspect of chemical reactivity due to the spin-polarization process, the atom-condensed SP-DFT Fukui indices, $f_{NS,k}^-$ and $f_{SS,k}^-$, are collected in Table 4. $f_{NS,k}^-$ is significant for obtaining an understanding of how the electron density is reorganized, whereas $f_{SS,k}^-$ provides information on the spin density reorganization when the system undergoes a spin-polarization process.

Positive and negative values of $f_{NS,k}^-$ can be interpreted following the operational formulas based on the finite-difference approximation as

$$f_{NS,k}^- \approx \left(\frac{\Delta\rho_k}{\Delta N_S}\right)_{N,v(\vec{r}),B(\vec{r})} \approx \frac{1}{2}(\rho_k^t - \rho_k^s) \qquad (17)$$

where ρ_k^t and ρ_k^s correspond to the electron densities at site k in the triplet and singlet states, respectively. Therefore, a positive value implies that $\rho_k^t > \rho_k^s$, indicating a charge depletion of site k under a spin-polarization process, whereas a negative value implies a charge accumulation on site k. The same analysis can be done for the $f_{SS,k}^-$ values: a positive value indicates a depletion of the spin density. As can be noted in Table 4, the β-carbon atom tends to accumulate electron charge when the intermediate decreases its spin number for those formed through an α-attack mechanism when $^3\pi\pi^*$ acrolein reacts with ethylene and methoxyethylene, whereas this center tends to deplete electron charge for the reaction with acrylonitrile. The opposite tendency is observed on the substituted carbon atom (C_1) of the olefins. In contrast, in the three cases studied, the intermediate produced by a β-attack mechanism shows the α-carbon atom to be prone to accumulate electron density whereas C_1 has the tendency to deplete electron density as the spin multiplicity decrease. Note that the centers that are highly susceptible for depletion and accumulation of electronic charge correspond to the interacting sites in the cyclization process.

From the values of $f_{SS,k}^-$, one can also see that the sites that are most likely to deplete spin density correspond to the interacting sites in the cyclization process, i.e., C_β and C_1 for the intermediates produced by an α path and C_α and C_1 for the intermediates formed by a β path.

On the other hand, we can note different values of both the $f_{NS,k}^-$ and $f_{SS,k}^-$ Fukui indices for the carbonyl O atom for the intermediates formed by α and β attacks. These values are higher in the species formed by the β path, which might be due to the fact that the radical on the α-carbon atom is delocalized on the C═O group. This result is in agreement with the work reported by Erickson and Kahn,[61] who established that electron delocalization drives the stabilization of the intermediate formed by a β mechanism.

The regioselectivity in the formation of cyclobutane derivatives is determined, on one hand, by the formation of the 1,4-biradical intermediate from the attack of $^3\pi\pi^*$ acrolein on an olefin. On the other hand, the cyclization process that takes place after the intersystem crossing also plays an

TABLE 5: Atom-Condensed SP-DFT Fukui Indices, $f^{-}_{NN,k}$, $f^{+}_{NN,k}$, and $f^{0}_{NN,k}$, of the 1,4-Biradical Intermediate Formed through the α and β Pathways for R1−R3 in the Singlet State[a]

	α Path					β Path			
	atom k	$f^{-}_{NN,k}$	$f^{+}_{NN,k}$	$f^{0}_{NN,k}$		atom k	$f^{-}_{NN,k}$	$f^{+}_{NN,k}$	$f^{0}_{NN,k}$
R1	O	0.0935	0.0570	0.0753	**R1**	O	0.1252	0.1466	0.1359
	C_α	0.0508	0.0180	0.0344		C_α	0.3065	0.2703	0.2884
	C_β	0.3347	0.3558	0.3453		C_β	0.0407	0.0211	0.0309
	C_1	0.4047	0.4163	0.4105		C_1	0.4197	0.4408	0.4302
	C_2	0.0234	0.0203	0.0218		C_2	0.0228	0.0154	0.0191
R2	O	0.0827	0.0463	0.0645	**R2**	O	0.1201	0.1420	0.1311
	C_α	0.0411	0.0189	0.0300		C_α	0.3080	0.2621	0.2850
	C_β	0.3286	0.3637	0.3461		C_β	0.0336	0.0196	0.0266
	C_1	0.3187	0.3417	0.3302		C_1	0.3188	0.3641	0.3414
	C_2	0.0141	0.0234	0.0187		C_2	0.0206	0.0250	0.0228
R3	O	0.1063	0.0508	0.0786	**R3**	O	0.1547	0.1472	0.1509
	C_α	0.0440	0.0166	0.0303		C_α	0.3066	0.2719	0.2892
	C_β	0.3349	0.3448	0.3399		C_β	0.0277	0.0177	0.0227
	C_1	0.2721	0.3112	0.2917		C_1	0.2694	0.3078	0.2886
	C_2	0.0206	0.0160	0.0183		C_2	0.0230	0.0125	0.0177

[a] Values obtained at the B3LYP/6-311G(d,p) level.

TABLE 6: Δf_{NN} Criterion to Evaluate the Local Hard−Soft Acid−Base Principle in the Cyclization Process[a]

	α path			β path			
reaction	$[C_1^+, C_\beta^-]$	$[C_1^-, C_\beta^+]$	$[C_1^0, C_\beta^0]$	$[C_1^+, C_\alpha^-]$	$[C_1^-, C_\alpha^+]$	$[C_1^0, C_\alpha^0]$	regioselectivity
R1	0.0816	0.0489	0.0652	0.1343	0.1494	0.1418	**HH**
R2	0.0131	0.0450	0.0159	0.0561	0.0567	0.0564	**HT**
R3	0.0237	0.0727	0.0482	0.0012	0.0025	0.0006	**HH**

[a] Notation used: $\Delta f_{NN} = |f^{\pm}_{NN,Ci} - f^{\mp}_{NN,Cj}| \equiv [C_i^{\pm}, C_j^{\mp}]$.

important role in the determination of the final **HH/HT** regioproduct ratio, as was pointed out by Wilsey et al.[8] Such a process can be seen as an intramolecular electronic reorganization on the interacting centers in the formation of the new bond. In this sense, the Fukui function should be used to investigate the regioselectivy of the [2 + 2] photocycloaddition reaction. Because the biradical intermediates present a singlet open-shell configuration, we used the generalized Fukui indices $f^{-}_{NN,k}$, $f^{+}_{NN,k}$, and $f^{0}_{NN,k}$ to characterize the local reactivity of the biradical intermediate upon cyclization. These values are collected in Table 5.

High values of $f^{-}_{NN,k}$ and $f^{+}_{NN,k}$ are associated with centers where the electron density is strongly depleted and accumulated, respectively, upon electrophilic and nucleophilic attacks, whereas a high value of $f^{0}_{NN,k}$ is associated with atoms that are more susceptible to radical attack. As can be observed from Table 5, the highest values correspond to the atoms involved in the cyclization reaction, i.e., C_1 and C_β for the intermediate formed by an α pathway and C_1 and C_α for the species produced by a β pathway, suggesting that the cyclization reaction can be treated as an electrophilic−nucleophilic event or a radical event. On the other hand, the carbonyl O atom shows a higher reactivity in intermediates formed through a β pathway than for those formed through an α pathway, reflecting again that the electron density is more delocalized.

Finally, to explain the regioselectivity, we invoked the softness-matching criterion corresponding to the local hard−soft acid−base principle.[62−64] This is based on the smallest absolute deviation between the local softness values of the interacting centers ($s_k^{\pm} = f_k^{\pm} S$, where S is the global softness). However, in the case of the intramolecular processes studied in the present article, the criterion can be reduced to the minimum absolute deviation between the Fukui indices, Δf_{NN}. This is given for the **HT** (or α) and **HH** (or β) pathways as

$$\Delta f_{NN} = |f^{\pm,0}_{NN,C_1} - f^{\mp,0}_{C_\beta}| \tag{18}$$

and

$$\Delta f_{NN} = |f^{\pm,0}_{NN,C_1} - f^{\mp,0}_{C_\alpha}| \tag{19}$$

respectively.

We examined the cyclization process of the intermediate in the singlet state as nucleophilic−electrophilic and radical intramolecular events. Table 6 collects the Δf_{NN} values. Note that the Δf_{NN} values for **R1** are higher than those for the other reactions, which might indicate that the cyclization process is less efficient than for the intermediates obtained in reactions with substituted alkenes. On the other hand, the intermediate formed in **R1** by an α mechanism presents a lower values of Δf_{NN} and was found to be less stable than that formed by a β mechanism. We also note that the cyclization process in the intermediates generated by substituted alkenes with electron-donating (**R2**) and electron-withdrawing (**R3**) groups show a significant preference for one of the cycloadducts. In the first case, the minimum values, taking both a nucleophilic−electrophilic and radical events, are observed for the species formed by an **HT** or α pathway, whereas in the second case, the most favorable interaction is to form the **HH** cyclobutane derivative, which is in agreement with the expected regioselectivity. It is interesting to stress that the complementary analysis carried out between the energy and reaction force concept together with the SP-DFT-based reactivity descriptors is suitable for gaining an understanding of the regioselectivity of the photocycloaddition reaction studied. This is especially the case for **R2**, where both regioisomers can be expected as products. Based on the energetic and reaction force criteria, the two mechanisms

prove to be more competitive. However, the SP-DFT response functions reveal the preference of one of the mechanisms to form the cyclobutane derivative.

5. Conclusions

In this article, we have presented a detailed study of the first step of the [2 + 2] photocycloaddition of triplet $\pi\pi^*$ acrolein to olefin in its ground state, i.e., the formation of a 1,4-biradical intermediate. This was done at the B3LYP/6-311+G(d,p) level of theory using ethylene, methoxyethylene, and acrylonitrile as model systems for which both kind of attacks, α and β pathways, were investigated. The results were rationalized in a complementary way between the reaction force concept and conceptual spin-polarized density functional theory. We found that the α pathway yields the **HT** regioisomer whereas the β pathway forms the **HH** regiosomer, with the β mechanism being the thermodynamically and kinetically most favorable path. For both types of reaction paths, a substituent effect was observed: Electron-rich and electron-poor alkenes increase the thermodynamic driving force and decrease the energy barrier with respect to the reaction between acrolein and ethylene. However, the two mechanisms are more competitive for the reaction between acrolein and methoxyethylene, where the formation of the **HT** regioproduct is also expected on the basis of the energy and reaction force criteria.

Complementarily, an analysis of the SP-DFT global and local response functions carried out on the biradical intermediate provided information on the capability of the system to change its spin multiplicity, i.e., the stabilization associated with an intersystem crossing. The analysis at the local level ($f^{-}_{\mathrm{NN},k}$ and $f^{-}_{\mathrm{SS},k}$) allows for the identification of how both the electron density and the spin density are reorganized in the direction of decreasing spin number. Finally, the regioselectivity in the formation of the cyclobutane derivative was explained in terms of the generalized Fukui indices, $f^{\pm,0}_{\mathrm{NN},k}$, and the local hard−soft acid−base principle based on the softness-matching Δf_{NN} criterion. Whereas reaction with an electron-rich alkene preferentially yields the **HT** regioisomer, reaction with an electron-poor alkene yields the **HH** regioproduct.

Acknowledgment. This work was support by a Visiting Postdoctoral Fellowship for P.J. from the Fund for Scientific Research Flanders (FWO). P.G. and F.D.P. thank FWO and VUB for continuous support of their research group. P.J. and A.T.-L. acknowledge FONDECYT (Chile) Project 1060590. All authors acknowledge the Chile−Flanders Bilateral Agreement.

References and Notes

(1) Schuster, D. I.; Lem, G.; Kaprinidis, N. A. *Chem. Rev.* **1993**, *93*, 3.
(2) Corey, E. J.; Bass, J. D.; LeMathieu, R.; Mitra, R. B. *J. Am. Chem. Soc.* **1964**, *86*, 5570.
(3) Eaton, P. E. *Acc. Chem. Res.* **1968**, *1*, 50.
(4) Hasting, D. J.; Weedon, A. C. *J. Am. Chem. Soc.* **1991**, *113*, 8525.
(5) Andrew, D.; Weedon, A. C. *J. Am. Chem. Soc.* **1995**, *117*, 5647.
(6) Broeker, J. L.; Eksterowicz, J. E.; Belk, A. J.; Houk, K. N. *J. Am. Chem. Soc.* **1995**, *117*, 1847.
(7) Suichi, T.; Shimo, T.; Somekawa, K. *Tetrahedron* **1997**, *53*, 3545.
(8) Wilsey, S.; Gonzalez, L.; Robb, M. A.; Houk, K. N. *J. Am. Chem. Soc.* **2000**, *122*, 5866.
(9) Bertrand, C.; Boequant, J.; Pete, J. P.; Humbel, S. *J. Mol. Struct. (THEOCHEM)* **2001**, *538*, 165.
(10) García-Expósito, E.; Bearpark, M. J.; Ortuño, R. M.; Robb, M. A.; Branchadell, V. *J. Org. Chem.* **2002**, *67*, 6070.
(11) García-Expósito, E.; Álvarez Larena, A.; Branchadell, V.; Ortuño, R. M. *J. Org. Chem.* **2004**, *69*, 1120.
(12) De Proft, F.; Fias, S.; Van Alsenoy, C.; Geerlings, P. *J. Phys. Chem. A* **2005**, *109*, 6335.
(13) Parr, R. G.; Yang, W. *Density Functional Theory of Atoms and Molecules*; Oxford University Press: New York, 1989.
(14) Chermette, H. *J. Comput. Chem.* **1999**, *20*, 129.
(15) Geerlings, P.; De Proft, F.; Langenaeker, W. *Chem. Rev.* **2003**, *103*, 1793.
(16) Geerlings, P.; De Proft, F. *Phys. Chem. Chem. Phys.* **2008**, *10*, 3028.
(17) Pérez, P.; Andrés, J.; Safont, V. S.; Tapia, O.; Contreras, R. *J. Phys. Chem. A* **2002**, *106*, 5353.
(18) Galván, M.; Vela, A.; Gázquez, J. L. *J. Phys. Chem.* **1988**, *92*, 6470.
(19) Vargas, R.; Galván, M.; Vela, A. *J. Phys. Chem. A* **1998**, *102*, 3134.
(20) Vargas, R.; Galván, M. *J. Phys. Chem.* **1996**, *100*, 14651.
(21) Melin, J.; Aparicio, F.; Galván, M.; Fuentealba, P.; Contreras, R. *J. Phys. Chem. A* **2003**, *107*, 3831.
(22) Pintér, B.; De Proft, F.; Van Speybroeck, V.; Hemelsoet, K.; Waroquier, M.; Chamorro, E.; Veszprémi, T.; Geerlings, P. *J. Org. Chem.* **2007**, *72*, 348.
(23) Oláh, J.; De Proft, F.; Veszprémi, T.; Geerlings, P. *J. Phys. Chem. A* **2004**, *108*, 490.
(24) Oláh, J.; Veszprémi, T.; Nguyen, M. T. *Chem. Phys. Lett.* **2005**, *401*, 337.
(25) Chamorro, E.; Santos, J. C.; Escobar, C. A.; Pérez, P. *Chem. Phys. Lett.* **2006**, *431*, 210.
(26) Rincón, E.; Pérez, P.; Chamorro, E. *Chem. Phys. Lett.* **2007**, *448*, 273.
(27) Oláh, J.; Veszprémi, T.; Proft, F. D.; Geerlings, P. *J. Phys. Chem. A* **2007**, *111*, 10815.
(28) Pérez, P.; Chamorro, E.; Ayers, P. W. *J. Chem. Phys.* **2008**, *128*, 204108.
(29) Cardenas-Jirón, G. I.; Gutiérrez-Oliva, S.; Melin, J.; Toro-Labbé, A. *J. Phys. Chem. A* **1997**, *101*, 4621.
(30) Toro-Labbé, A. *J. Phys. Chem. A* **1999**, *103*, 4398.
(31) Jaque, P.; Toro-Labbé, A. *J. Phys. Chem. A* **2000**, *104*, 995.
(32) Pérez, P.; Toro-Labbé, A. *J. Phys. Chem. A* **2000**, *104*, 1557.
(33) Chattaraj, P. K.; Gutiérrez-Oliva, S.; Jaque, P.; Toro-Labbé, A. *Mol. Phys.* **2003**, *101*, 2841.
(34) Martínez, J.; Toro-Labbé, A. *Chem. Phys. Lett.* **2004**, *392*, 132.
(35) Toro-Labbé, A.; Gutiérrez-Oliva, S.; Concha, M.; Murray, J. S.; Politzer, P. *J. Chem. Phys.* **2004**, *121*, 4570.
(36) Politzer, P.; Toro-Labbé, A.; Gutiérrez-Oliva, S.; Herrera, B.; Jaque, P.; Concha, M.; Murray, J. S. *J. Chem. Sci.* **2005**, *117*, 467.
(37) Gutiérrez-Oliva, S.; Herrera, B.; Toro-Labbé, A.; Chermette, H. *J. Phys. Chem. A* **2005**, *109*, 1748.
(38) Politzer, P.; Burda, J. V.; Concha, M.; Lane, P.; Murray, J. S. *J. Phys. Chem. A* **2006**, *110*, 756.
(39) Rincón, E.; Jaque, P.; Toro-Labbé, A. *J. Phys. Chem. A* **2006**, *110*, 9478.
(40) Herrera, B.; Toro-Labbé, A. *J. Phys. Chem. A* **2007**, *111*, 5921.
(41) Burda, J. V.; Toro-Labbé, A.; Gutiérrez-Oliva, S.; Murray, J. S.; Politzer, P. *J. Phys. Chem. A* **2007**, *111*, 2455.
(42) Toro-Labbé, A.; Gutiérrez-Oliva, S.; Murray, J. S.; Politzer, P. *Mol. Phys.* **2007**, *105*, 2619.
(43) Parr, R. G.; Donnelly, R. A.; Levy, M.; Palke, W. E. *J. Chem. Phys.* **1978**, *68*, 3801.
(44) Parr, R. G.; Pearson, R. G. *J. Am. Chem. Soc.* **1983**, *105*, 7512.
(45) Chamorro, E.; Pérez, P.; De Proft, F.; Geerlings, P. *J. Chem. Phys.* **2006**, *124*, 044105.
(46) Parr, R. G.; von Szentpaly, L.; Liu, S. *J. Am. Chem. Soc.* **1999**, *121*, 1922.
(47) Parr, R. G.; Yang, W. *J. Am. Chem. Soc.* **1984**, *106*, 4049.
(48) Contreras, R.; Fuentealba, P.; Galván, M.; Pérez, P. *Chem. Phys. Lett.* **1999**, *304*, 405.
(49) Yang, W.; Parr, R. G.; Pucci, R. *J. Chem. Phys.* **1984**, *81*, 2862.
(50) Chamorro, E.; Pérez, P. *J. Chem. Phys.* **2005**, *123*, 114107.
(51) Born, M.; Oppenheimer, J. R. *Ann. Phys.* **1927**, *84*, 457.
(52) Fukui, K. *Acc. Chem. Res.* **1981**, *14*, 363.
(53) Becke, A. D. *J. Chem. Phys.* **1993**, *98*, 5648.
(54) Lee, C.; Yang, W.; Parr, R. G. *Phys. Rev. B* **1998**, *37*, 785.
(55) Krishnan, R.; Binkley, J. S.; Seeger, R.; Pople, J. A. *J. Chem. Phys.* **1980**, *72*, 650.
(56) Clark, T.; Chandrasekhar, J.; Schleyer, P. *J. Comput. Chem.* **1983**, *4*, 294.
(57) Frisch, M. J.; Trucks, G. W.; Schlegel, H. B.; Scuseria, G. E.; Robb, M. A.; Cheeseman, J. R.; Montgomery, J. A., Jr.; Vreven, T.; Kudin, K. N.; Burant, J. C.; Millam, J. M.; Iyengar, S. S.; Tomasi, J.; Barone, V.; Mennucci, B.; Cossi, M.; Scalmani, G.; Rega, N.; Petersson, G. A.; Nakatsuji, H.; Hada, M.; Ehara, M.; Toyota, K.; Fukuda, R.; Hasegawa, J.; Ishida, M.; Nakajima, T.; Honda, Y.; Kitao, O.; Nakai, H.; Klene, M.; Li, X.; Knox, J. E.; Hratchian, H. P.; Cross, J. B.; Bakken, V.; Adamo, C.; Jaramillo, J.; Gomperts, R.; Stratmann, R. E.; Yazyev, O.; Austin, A. J.; Cammi, R.; Pomelli, C.; Ochterski, J. W.; Ayala, P. Y.; Morokuma, K.; Voth, G. A.; Salvador, P.; Dannenberg, J. J.; Zakrzewski, V. G.; Dapprich, S.; Daniels, A. D.; Strain, M. C.; Farkas, O.; Malick, D. K.; Rabuck, A. D.; Raghavachari, K.; Foresman, J. B.; Ortiz, J. V.; Cui, Q.; Baboul, A. G.; Clifford, S.; Cioslowski, J.; Stefanov, B. B.; Liu, G.; Liashenko, A.; Piskorz, P.; Komaromi, I.; Martin, R. L.; Fox, D. J.; Keith, T.; Al-Laham, M. A.;

Peng, C. Y.; Nanayakkara, A.; Challacombe, M.; Gill, P. M. W.; Johnson, B.; Chen, W.; Wong, M. W.; Gonzalez, C.; Pople, J. A. *Gaussian 03*, revision D.01; Gaussian, Inc.: Pittsburgh, PA, 2004.

(58) González, C.; Schlegel, H. B. *J. Phys. Chem.* **1990**, *94*, 5523.

(59) Seeger, R.; Pople, J. A. *J. Chem. Phys.* **1977**, *66*, 3045.

(60) Bauernschmitt, R.; Ahlrichs, R. *J. Chem. Phys.* **1996**, *104*, 9047.

(61) Erickson, J. A.; Kahn, S. D. *Tetrahedron* **1993**, *49*, 9699.

(62) Gázquez, J. L.; Méndez, F. *J. Phys. Chem.* **1994**, *98*, 4591.

(63) Geerlings, P.; De Proft, F. *Int. J. Quantum Chem.* **2000**, *80*, 227.

(64) Damoun, S.; de Woude, G. V.; Méndez, F.; Geerlings, P. *J. Phys. Chem. A* **1997**, *101*, 886.

JP807754F